Ultrasonics Sonochemistry 111 (2024) 107121

Contents lists available at ScienceDirect

Ultrasonics Sonochemistry

journal homepage: www.elsevier.com/locate/ultson

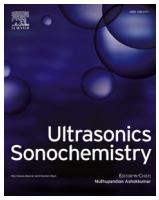

Effects of Ultrasound on Reactive Crystallization and Particle Properties of an Aromatic Amine in Batch and Continuous modes

Biyu Zhang [a], Ida Ådnebergli [b], Georgios D. Stefanidis [c], Tom Van Gerven [a,*]

[a] Department of Chemical Engineering, Process Engineering for Sustainable Systems, KU Leuven, Celestijnenlaan 200F, 3001 Heverlee, Belgium
[b] Chemical Process Development, GE HealthCare, Lindesnesveien 208, 4521 Spangereid, Norway
[c] School of Chemical Engineering, Department of Process Analysis and Plant Design, National Technical University of Athens, Iroon Polytecneiou 9, Zografou 15780, Athens, Greece

ARTICLE INFO

Keywords:
Ultrasound
Reactive crystallization
Batch crystallization
Continuous crystallization
Particle properties
Particle size distribution

ABSTRACT

Ultrasound has shown its benefits in the manufacturing processes of many pharmaceuticals and fine chemicals. This study focused on the reactive crystallization system of an aromatic amine and explored the potential uses of ultrasound in both batch and continuous modes. In batch experiments, we studied the effects of different sonication conditions including power, duration, and starting point on final particle properties. Under ultrasound, the crystal form and crystal morphology remained well maintained. The results of particle size and size distribution suggested that ultrasound reduced the mean sizes by improving the nucleation process and breaking up large particles. Additionally, the presence of ultrasound in continuous experiments was capable of inducing nucleation and the crystal products collected had a suitable distribution. Integrating ultrasound into the beginning of the continuous crystallization process can be an alternative to the seeding technique. The increasing sonication power did not reduce the induction time substantially. This indicated that a rational sonication condition should balance the overall process efficiency and energy consumption. The findings from batch and continuous experiments indicate that ultrasound could intensify industrial crystallization of the aromatic amine. Incorporating energy-efficient ultrasound with the continuous process will potentially lead to increased production efficiency and a well-controlled product quality.

1. Introduction

Crystallization is one of the most important separation and purification processes particularly in the pharmaceutical industry and fine chemicals. The continuous supply of crystal products with a high and reproducible quality requires the crystallization process to be efficient and robust enough. Therefore, a desired industrial crystallization process has to yield high-quality products in terms of the final particle properties, such as crystal form, crystal morphology, crystal size, and size distribution [1–3]. Understanding the fundamentals of nucleation and crystal growth and the formation of final products plays a decisive role in the design of the operation conditions of the crystallization process.

Ultrasound has shown its benefits as a process intensification technique in the crystallization process of many compounds. The application of ultrasound has been proven to influence the crystallization process in many aspects such as enhancing nucleation [4–6], controlling particle size distribution [7–10], and polymorph control [4,11,12]. Extensive research was performed on applying ultrasound in the cooling crystallization system. Hatkar et al. applied ultrasonic irradiations into the cooling crystallization of sodium acetate where irradiation was applied when cooling was started. The sonicated experiments revealed that intentional seeding can be avoided in the presence of ultrasonic irradiation and the ultrasound operating parameters such as irradiation time and dissipated power affected the final particle properties [13]. Similar results were found by Narducci et al. who studied the ultrasound-assisted cooling crystallization of adipic acid. A short ultrasonic burst was used at the beginning of the cooling process and a growth-dominated process was achieved, resulting in crystal products with the desired regular hexagonal shape and unimodal size distribution [10]. Jordens et al. introduced ultrasound with different frequencies to the cooling crystallization of paracetamol, and found that the lower ultrasonic frequencies are preferable both to enhance the nucleation rate and to limit degradation [14]. These studies all suggest that ultrasound can

* Corresponding author.
E-mail address: tom.vangerven@kuleuven.be (T. Van Gerven).

https://doi.org/10.1016/j.ultsonch.2024.107121
Received 5 June 2024; Received in revised form 19 September 2024; Accepted 20 October 2024
Available online 22 October 2024
1350-4177/© 2024 The Author(s). Published by Elsevier B.V. This is an open access article under the CC BY-NC license (http://creativecommons.org/licenses/by-nc/4.0/).

benefit the cooling crystallization process and many sonication parameters have been studied to optimize ultrasound-assisted cooling crystallization systems.

Reactive crystallization, the combination of reaction and crystallization, is another form of crystallization. The operation of reactive crystallization can be done without the integration of the thermal energy that is required for cooling crystallization [15]. However, compared to ultrasound-assisted cooling crystallization, the literature on the combination of ultrasound with reactive crystallization is relatively few. Guo et al. applied ultrasound to the reactive crystallization of $BaSO_4$ and found that ultrasonic energy input had a significant impact on the induction time [16,17]. The study of Chen et al. proposed that the presence of ultrasound increased the reactive crystallization rate of vanadium in an acidic ammonium salts crystallization system by enhancing the collision frequency between NH_4^+ and vanadium ions [18]. Ma et al. introduced pulsed ultrasound into the reactive crystallization of lithium carbonate and found that pulsed ultrasound could increase the reaction rate and improve the particle size distribution [19]. Works investigating the application of ultrasound on reactive crystallization systems are still limited.

To apply ultrasound in a crystallization process, both sonicated reactor and sonication parameters have to be well designed. Adamou et al. [20] and Banakar et al. [21] review that ultrasound can be applied through various sono-chemical setups in batch and continuous processes. They also point out the effects of sonication parameters, such as frequency, power, and duration. For a reactive crystallization system, which happens usually very fast due to chemical reactions, it's even more challenging to control the crystallization process and the product properties. Therefore, more experimental studies are needed to reveal the influence of ultrasound in the reactive crystallization process, especially in terms of the design of the sonication conditions.

This work used an Aromatic Amine as a model compound and focused on its reactive crystallization process, aiming to address the industrial challenge of reducing manufacture time while maintaining product quality. The potential of ultrasound to intensify this reactive crystallization process was explored in both batch and continuous experiments, emphasizing its influence on the crystallization process and final particle properties. Different sonication conditions were adopted to find out how to integrate ultrasound into this crystallization system appropriately.

2. Material and Methods

2.1. Chemicals

The studied compound Aromatic Amine (written as AA below) with a purity of 99% was received in dry solid form from GE HealthCare. Ultrapure water (18.2 MΩ·cm) and methanol (99.9% purity, Merck Life Science) were mixed at a 2:1 ratio by volume as solvent. NaOH (50 wt%, Merck Life) was used to dissolve the compound and get an anionic solution with the desired concentration of 25 wt%. HCl (17.5 wt%, diluted from HCl of 37%, Merck Life) as the other reactant was used to neutralize the system and further obtain the protonated crystals. Acetonitrile (99.9% purity, Merck Life) was used as the dispersant during the measurements of particle size distribution (PSD).

2.2. Experimental setup

In this work, two setups were built for batch crystallization and continuous nucleation of AA, respectively, shown in Fig. 1. Inspired by a sonicated crystallizer for the precipitation of manganese carbonate developed by Jordens et al. [22], the batch setup is built up as follows. The double-jacket crystallizer with a volume of 310 mL is glued to a Langevin-type transducer from Ultrasonics World (MPI-7850D-20_40_60H, non-focused, diameter: 78 mm) at the bottom. Ultrasound frequency and amplitude are regulated using a Waveform Generator (Picotest G5100A) and an Amplifier (E&I 1020L RF power amplifier), and the resonance frequency (41 ± 1 kHz) is determined by an Impedance Analyzer (SinePhase Impedance Analyzer 16777 k) beforehand. Table 2 lists the resonance frequency and the amplitude applied in this study. On the top is a glass lid which has five holes for the mechanical stirrer in the center and the condenser (not shown in the figure), the pH probe connected to a pH meter (VWR pH 1000L), the type-K thermocouple connected to a Pico TC-08 thermocouple data logger, and the HCl addition opening in the surrounding. A thermostat bath (Lauda Eco RE 620 S) is used to maintain the desired crystallization temperature.

Inspired by the flow setup developed by Vancleef et al. [23] and Hussain et al. [12], in this work, the continuous crystallization setup consists of the following parts: two inlet parts for reactants AA and HCl (PFA tube), a three-way valve, a connection section of 5 cm (PFA tube), a flow reactor of 16 cm (glass tube, 1.13 mL in volume), and an outlet section of 5 cm. The flow reactor is placed in a rectangular glass housing which is connected to a Julabo HE Lab thermostat for temperature control. The transducer (Ultrasonics World, MPI-7850D-20_40_60H) is attached to the bottom of the glass housing to sonicate the reactor. Ultrasound frequency and amplitude are regulated the same way as above. A syringe pump (Chemyx, Fusion 4000, pump rates from 0.5109 μL/min to 121.4 mL/min) equipped with a 50 mL Terumo® syringe is used to pump the other reactant HCl. A pulse-free gear pump (Ismatec Reglo-Z digital, Z186 pump head, pump range from 0.0985 mL/min to 9.85 mL/min) is used to pump the solution AA. The solution AA flows through a tubing coil placed in a water tank to reach the desired temperature. Two type-K thermocouples connected to a Pico TC-08 thermocouple data logger are used for tracking the temperature, respectively at the outlet of the tubing coil and the outlet of the reactor. The thermocouple placed at the inlet originally was removed because it

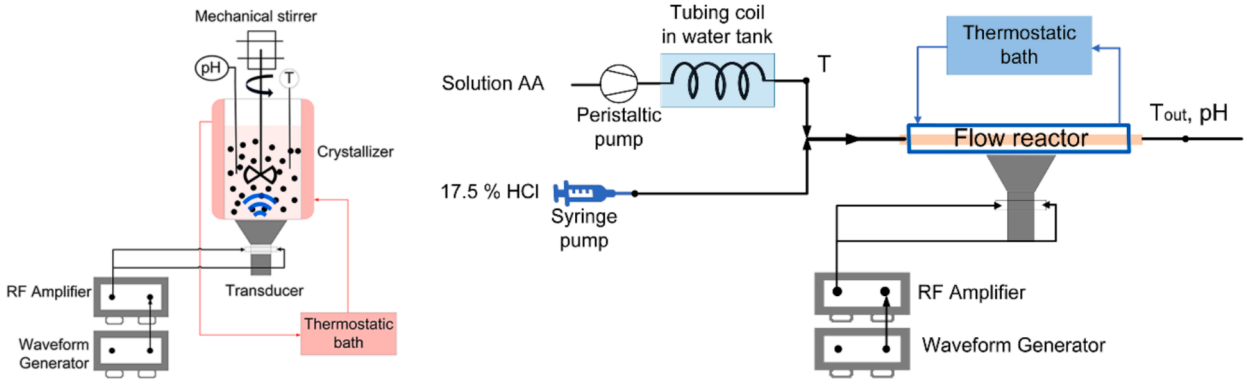

Fig. 1. Left: setup for batch crystallization experiments. Right: setup for continuous nucleation experiment. In the flow setup, two nodes "T" and "T_{out}, pH" indicate the positions of measuring inlet temperature, outlet temperature and pH, respectively.

was tested to cause severe scaling problems. The outlet temperature of the reactor was tested to maintain at the desired temperature. pH was given by manually measuring the pH of the collected mixture at the outlet. A vacuum filtration setup (a Pyrex™ Borosilicate glass filter flask with a 0.22 μm filter membrane, connected to a VacuuBrand® vacuum pump) was placed at the end to filter the outflowing slurry and collect the crystals.

2.3. Experimental procedure

2.3.1. Batch experiments

The chemical reaction involved in this study is a neutralization reaction, similar to the precipitation of L-Glutamic Acid (LGA) by mixing sodium L-glutamate ($NaGlu{\cdot}H_2O$) and sulfuric acid (H_2SO_4) [24], following Eq. (1). The equilibrium between LGA solid and its soluble form follows Eq. (2):

$$NaGlu \bullet H_2O\ (l) + \frac{1}{2}H_2SO_4\ (l) \Leftrightarrow\ H \bullet Glu\ (l) + \frac{1}{2}Na_2SO_4\ (l) \quad (1)$$

$$H \bullet Glu\ (l) \Leftrightarrow^{K_{sp}} H \bullet Glu\ (s) \quad (2)$$

$H \bullet Glu$ (l) and $H \bullet Glu$ (s) are the soluble form and solid form of L-glutamic acid, respectively. Similarly, the reactive crystallization of the studied aromatic amine occurs by mixing its sodium salt form with an acid, as described by the reaction: $AA^- + H^+ \rightarrow AA\ (l) \rightarrow AA\ (s)$. In this process, the crystallization of AA was initialized by adding HCl to the anionic solution forming a neutralized slurry and driven by the decrease in pH. In principle, the crystals appear when the concentration of AA exceeds its solubility.

In the batch experiments, the solution AA of 25 wt% was prepared beforehand and 200 mL was pumped into the reactor for each experiment. A 15-minute neutralization period followed by a 15-minute holding period was employed. HCl (17.5 wt%) was manually introduced in four stages at five-minute intervals over the 15-minute neutralization period, following a defined protocol to achieve a consistent pH-changing curve shown in Fig. 2. The traditional silent (without ultrasound) and ultrasound-assisted crystallization experiments were performed at a constant temperature of 60 °C for 30 min. Both addition of HCl and sonication effect would increase the temperature. Under the influence of thermostat, the temperature was kept at 60 (±2) °C, shown in Fig. 2. All batch sonicated experiments were conducted at a resonance frequency of 40 (±1) kHz. The input sonication power was characterized by the calorimetry method described in Section 2.4. The silent experiments were triplicated as a reference, and the sonicated experiments were conducted two times under different sonicated conditions, which included different sonication powers, durations, and starting points.

After crystallization, a pressure filtration equipment (BHS, Pocket Leaf Filter) connected to nitrogen was used to filter the slurry. 200 mL slurry was divided into 2 times of filtration and the same slurry volume of 100 mL was filtered each time to obtain a 15–25 mm filter cake. The filtration time was recorded by a stopwatch. The average of two measured filtration times was used to evaluate the filterability. Then the filter cake was transferred to an IKA® heating plate and heated to dry under 120 °C in the fume hood. After 2-hour heating and at least 24-hour air drying in the fume hood, the particles were ready for post-analysis involved yield calculation, crystal form determination using FTIR, particle shape visualization via SEM, and PSD measurements using Malvern Hydro SV.

The crystallization yield was calculated based on the dissolved AA, as Eq. (3),

$$\text{Yield } \% = \frac{\text{Weight of particles collected after drying}}{\text{Weight of solids initially dissolved in that volume}} \times 100\% \quad (3)$$

The crystal form was characterized via Attenuated Total Reflection – Fourier Transform Infrared (ATR-FTIR) spectroscopy (Perkin-Elmer Spectrum 100 with UATR accessory) and confirmed by comparing the spectra of the products obtained from crystallization experiments with the industrially produced materials. The particle shape was visualized using a Scanning Electron Microscope (SEM, JEOL JSM – 6010 L V) after coating the samples with a gold/palladium coating using a JEOL JFC 1300 sputter coater (40 mA for 30 s). PSD was analyzed using a Malvern (Mastersizer 3000 – Hydro SV) with acetonitrile as the dispersant. The stirring speed was set at 1500 rpm. Three samples were taken for each experimental product and measured independently, so the average of the three measurements was delivered as the PSD result.

2.3.2. Continuous experiments

In the continuous mode, the two reactants – solution AA and HCl were pumped into the reactor. Different flow rate ratios of solution AA and HCl were employed, shown in Table 1. All flow experiments were executed three times. Solution AA was always pumped in first for 5–10 min to rinse the setup and to reach a stable outlet temperature when HCl was ready to flow in. The timing of the induction process was started using a stopwatch once HCl was pumped into the reactor. In the meantime, ultrasound was applied (only in the sonicated experiments.)

Table 1
Flow conditions.

AA flow rate (mL/min)	HCl flow rate (mL/min)	Flow ratio of AA and HCl	Total flow rate (mL/min)	Residence time (s)
2.5200	0.1890	100:7.5	2.709	25.0(±0.2)
	0.2016	100:8.0	2.721	
	0.2142	100:8.5	2.734	

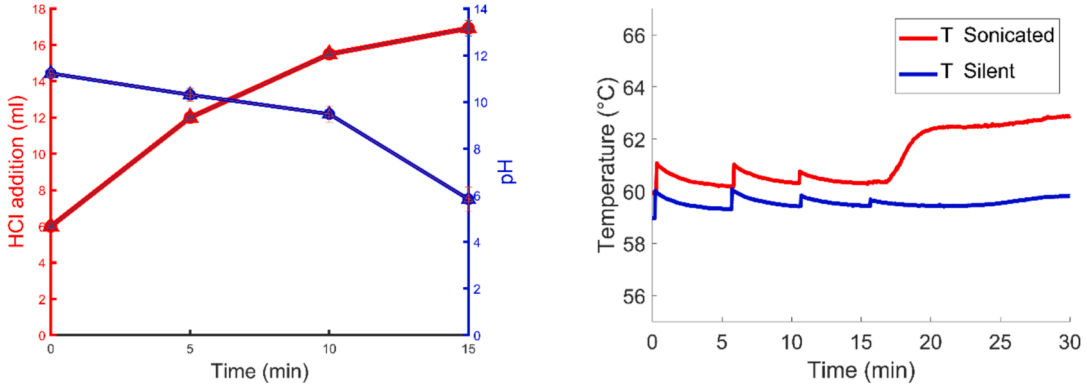

Fig. 2. Left: HCl addition protocol and pH-changing curve. The data points are the average of ten experiments and the error bars are the standard deviation. Right: examples of temperature recording in the sonicated and silent batch crystallization experiments.

From this point, the time until the first crystals was visually detected in the flow reactor by naked eye was registered, which was defined as the induction time. The visual detection of crystals was shown as a reliable method for noticing crystallization [25,26]. The induction time under both silent and sonicated flow was measured, and the effects of flow ratio and sonication power were studied.

The outflowing product slurry was collected for 2–3 min and the experiment was stopped. A long collection time was not applied for the following reasons: a) the filtration rate of the present vacuum setup was limited, b) the slurry layer that cannot be filtered within a reasonable time frame continued to crystallize. The collected crystals were allowed to dry for at least 24 h in the fume hood. Then the crystal shape and size were measured via SEM and Malvern following the same procedure as described in Section 2.3.1. In case no nucleation was observed after 8 min, the experiment was stopped, because long induction times are generally undesired for continuous crystallizers.

2.4. Sonication conditions

The actual sonication power dissipated in the system was determined by a calorimetric method [27,28], by measuring the rate of temperature increase. The calorimetric technique assumes that the ultrasonic energy delivered to the system is converted into heat. In this work, ultra-pure water was used as the sonicated medium to measure the calorimetric power in both batch and flow system. The temperature was monitored via thermocouples and three separate measurements were performed for each experimental condition. The calorimetric power was calculated according to Eq. (4),

$$P_{cal} = mC_p\left(\frac{dT}{dt}\right)_{t=0} \quad (4)$$

where m and Cp are the mass (kg) and heat capacity (J/kg·K) of water, respectively. And $\left(\frac{dT}{dt}\right)_{t=0}$ is the initial slope of the increasing rate of temperature (K/s). Here, the initial heating rate was applied because it was not influenced by the initial bulk temperature of the water and the height of water in the vessel [29].

The input power per unit of volume, a key parameter used for scale-up [6], calculated as the input power divided by the volume of the solution, is used as the sonication power parameter in this study.

Table 2 gives the electrical powers applied in both batch and flow systems and the corresponding measured calorimetric powers, together with the frequency and amplitude of the ultrasound regulated by the Waveform Generator.

In the batch experiments, the sonication conditions (Fig. 3) varied in three aspects: a) sonication powers of 8.4 W/L, 22.6 W/L, and 36.3 W/L, with the same duration of 15 min and the same sonication starting point (when pH reached 7); b) sonication durations of 5 min and 15 min, with the same sonication power 22.6 W/L and the same sonication starting point (pH 7); c) sonication starting point – starting sonication at pH 10, pH 7, and 5 min before the end of experiments (the final 5 min), with the same sonication power of 22.6 W/L and duration of 5 min. In continuous experiments, the sonication conditions varied in sonication powers of 93.4, 165.9, and 216.5 W/L.

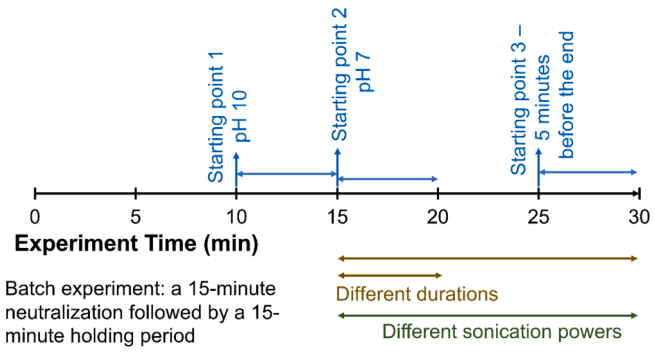

Fig. 3. Schematic diagram of sonication conditions of batch experiments.

3. Results and Discussion

3.1. Batch experiments

3.1.1. Stability of AA under ultrasound

Ultrasound has been shown to enable the transition from one to another form for some compounds [4,12,30]. However, the effect of the said technique still varies from compound to compound. The effect of ultrasound on the AA in this investigation was studied by comparing the ATR-FTIR spectra of the crystalline solids obtained from both the silent and sonicated experiments with the spectrum of industrially produced particles. Six samples from sonicated products and three samples from silent products were analyzed. One can see an example in Fig. 4, all spectra exhibited the same morphology, indicating that ultrasound had no discernible effect on the crystal form of compound AA.

Other than crystal form, the particles produced at silent and sonicated conditions possessed a similar porous ball-like morphology. As an example, the SEM images at the sonication powers of 8.4 W/L and 36.3 W/L and the silent condition are shown in Fig. 5. On the left side of this figure (pictures with the same magnification), it can be seen that the morphology of compound AA did not change under sonication. The right side of this figure indicates that sonicated samples had a smaller average size than silent ones, which was confirmed via PSD measurements reported in section 3.1.3. The exploration of the crystal growth mechanism is outside of the scope of this paper and will be reported in due course. Three possible explanations for the formation of this ball-like morphology are under investigation: a) spiral growth of the initial crystal face, b) agglomeration of small crystals, and c) the combination of both.

3.1.2. Yields calculation

Ultrasound can potentially enhance the crystallization process and achieve a higher yield in the manufacturing of many compounds

Table 2
Calorimetric power measurements.

	Flow rate (mL/min)	RT (s)[1]	Frequency (kHz)	Amplitude (mVpp)	Electrical power (W)[2]	Average calorimetric power (W)[3]	Standard deviation	P_{cal}/Volume (W/L)[4]
Batch (200 mL)	\		41.15	250	5	1.69	0.51	8.4
	\	\	41.15	500	12	4.51	0.32	22.6
	\	\	41.15	800	20	7.25	0.42	36.3
Flow (1.13 mL)	2.72	24.9	41.9	210	5	0.11	0.007	93.4
			41.9	300	10	0.19	0.008	165.9
			41.9	360	15	0.24	0.002	216.5

[1] RT: residence time.
[2] Electrical power refers to the power parameter on the Ultrasound Waveform Generator.
[3] Average of three measurements of calorimetric power.
[4] Input power per unit of volume is used as the sonication power parameter in this study.

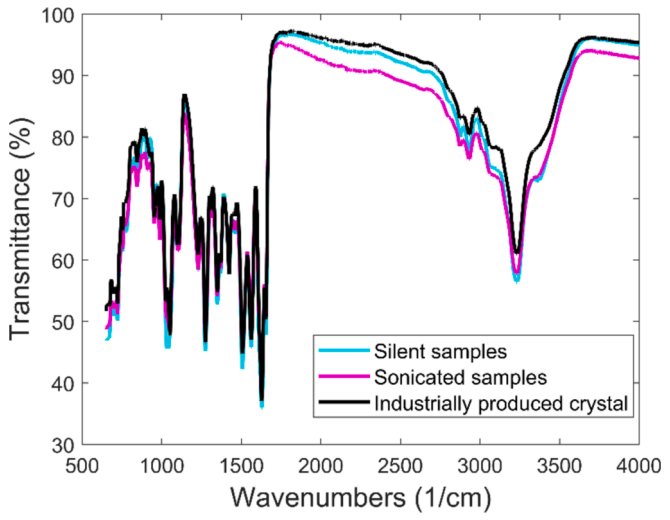

Fig. 4. An example of ATR-FTIR spectra of crystals from silent and sonicated experiments, and industrially produced crystals.

[31,32]. In this work, the effects of various sonication powers on the reactive crystallization yields of AA were evaluated. Ultrasound was introduced after pH reached 7 and always had the same duration of 15 min (holding time). Fig. 6 shows that the sonicated experiments achieved an average yield of 79% whereas the silent ones only achieved 43%, which revealed that sonication intensified this reaction and crystallization rates and led to higher yields of AA. According to the observation of the experimental crystallization process, ultrasound enhanced the secondary nucleation in the early stage of sonication thus increasing the overall crystallization rates and leading to higher yields. Moreover, there was not too much difference in yields among different sonication powers, which means that the system reached maximum yields after 15 min of sonication even when the power was low. From the perspective of rational use of ultrasound, excessive powers are not desired.

3.1.3. Particle size distribution

The particle sizes and the particle size distribution under both silent and various sonicated conditions were measured offline to analyze further the effects of ultrasound. Volume distributions of particle sizes are provided in Figs. 7–9 while the Dx10, Dx50, and Dx90 results are provided in Table 3. One can see that the sonicated samples were always smaller than the silent ones, which was expected from the SEM data. Fig. 7 showed that the silent sample had a bimodal distribution, while all of the sonicated samples had unimodal distribution. The transition of distribution from bimodal in silent mode to unimodal in sonicated mode indicates that almost no large particles appeared and the number of small particles increased under ultrasound. The large peak of the silent sample was located around 127 μm, while the peak of sonicated samples reached a minimum around 25 μm at the sonication power of 36.3 W/L. With the same duration of 15 min and the same sonication starting point of pH 7, the more powerful sonication led to smaller particles on average. One may expect that the presence of ultrasound could influence the crystallization process of compound AA by favoring nucleation, inhibiting crystal growth, or boosting deagglomeration. The effects of sonication duration and starting point were also investigated. As shown in Fig. 8, the samples from the experiments with different sonicated durations presented a similar unimodal distribution. The peak shifted from around 38 μm to around 27 μm as the sonication duration increased from 5 min to 15 min, which revealed the longer the sonicated duration, the smaller the particle size became. Similar to the PSD results from previous experiments, all experimental samples under the conditions of different sonication starting points had a unimodal size distribution (Fig. 9). The peak of the samples obtained under the sonication starting point of pH 7 was located around 38 μm, while the samples obtained under the sonication starting point of pH 10 showed the narrowest span with a close peak at around 35 μm. The nucleation process started at a pH of ca. 10, while a pH of 7 was a complete neutralization pH. Introducing ultrasound at the earlier stage of pH 10 significantly enhanced the nucleation and then nucleation dominated the crystallization process, leading to the product with many fines and a narrow span. In comparison, crystallization already occurred before pH reached 7 as the additions of HCl. Introducing ultrasound at a later stage (pH 7) both influenced the particles already crystallized and enhanced the secondary nucleation as well. Furthermore, from Fig. 9 and Table 3, the size distribution of the samples obtained under the condition of starting ultrasound at 5 min before the end of the experiment exhibited a peak at the minimum size of 19 μm and a span of 2.25. Combined with the size distribution of the silent sample – a similar span of 2.42 while the small peak was at 15 μm and the high peak was at 127 μm, one may conclude that 5-minute sonication at the end of the experiment affected the large particles by deagglomeration and resulted in a change in peak shape. Even though the same sonication power and duration were applied, starting ultrasound at different pH points can make a substantial difference in the crystallization process. Therefore, the combination of different sonication conditions, such as applying a short burst of ultrasound in the beginning to enhance the nucleation, not involving ultrasound until the neutralization is completed, and applying the ultrasound with moderate power and duration at the end of crystallization, would be considered to be optimal for an intensified crystallization and controlled particle size property.

A comprehensive analysis of PSD results from all sonicated conditions confirmed the role of ultrasound in increasing nucleation rate and deagglomeration, but which stage or stages of nucleation, crystal growth, and (de-)agglomeration were predominantly influenced was not clear. This reactive crystallization process in batch experiments was very intense as seen from the transition from a clear solution to a milky slurry, which made it very difficult to analyze the crystallization process accurately only by offline measurements. An in-depth study of kinetics with the aid of PAT tools is ongoing for a better understanding of the process.

3.1.4. Filtration behavior

This work evaluates the filterability of crystal products. It compares the filtration time of a slurry volume of 100 mL under the same filtration conditions. Table 3 gives the results. One can see that the silent sample had the shortest filtration time, implying that it behaved best on filtration. This is due to its larger average size of particles compared to the sonicated samples (almost two to three times on Dx50). Of all the sonicated experiments, the slurry from the 5 mins after pH 10' experiment filtered the quickest. The slurry from the '5 mins before the end' experiment was the slowest. This phenomenon can be explained by the particle size and distribution (Table 3, Figs. 7–9). The particles obtained under '5 mins after pH 10' were best in terms of size distribution: they were uniform, without humps. In contrast, the particles obtained under '5 mins before the end of the experiment' exhibited the widest span and smallest sizes. To conclude, ultrasound affects particle size and particle size distribution. This, in turn, influences the filterability of the produced slurry. Specifically, the decrease in sizes under sonication leads to a longer filtration time. Still, ultrasound shows the potential to offset this loss by narrowing down the span and producing more uniform products.

3.2. Continuous experiments

3.2.1. Induction time at different flow ratios

The continuous experiments started with the silent flow experiments without ultrasound as a reference. In the batch experiments, nucleation happened after 15 mL HCl was added into 200 mL solution AA. The same concentrations of AA and HCl were used in batch and flow experiments. Therefore, the first flow rate ratio of AA and HCl in the continuous

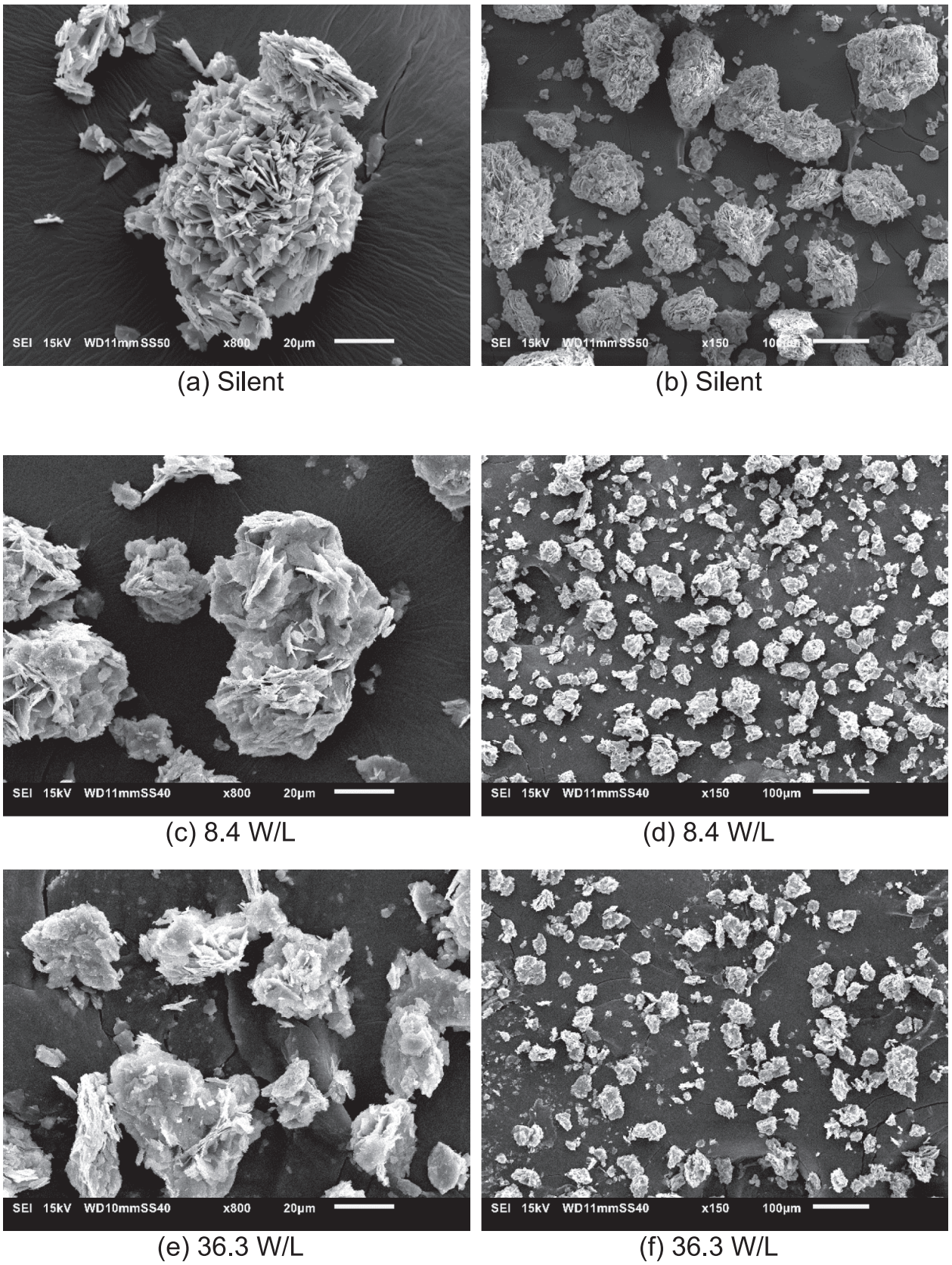

Fig. 5. SEM images of samples from (a-b) silent experiments, (c-d) sonicated experiments with power of 8.4 W/L, (e-f) sonicated experiments with power of 36.3 W/L.

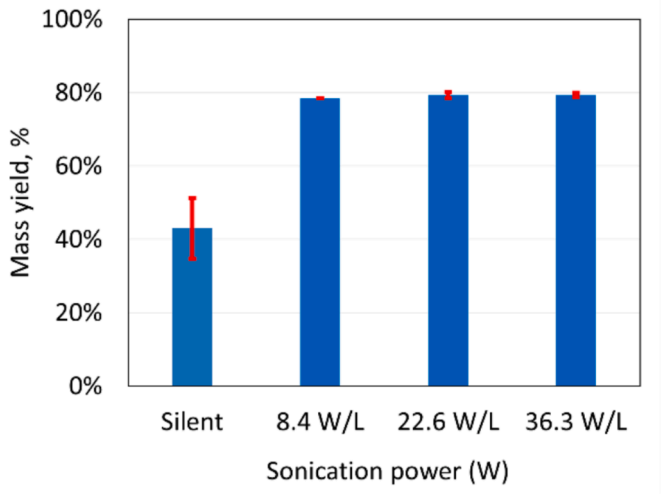

Fig. 6. Calculated yields for batch experiments under silent and different sonication powers. The bars represent the average of duplicated experiments, and the error bars represent the standard deviation.

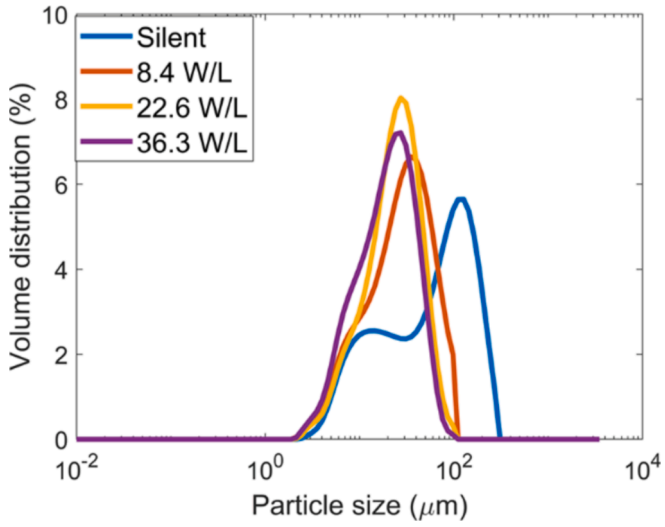

Fig. 7. Particle size volume distribution at different sonication powers.

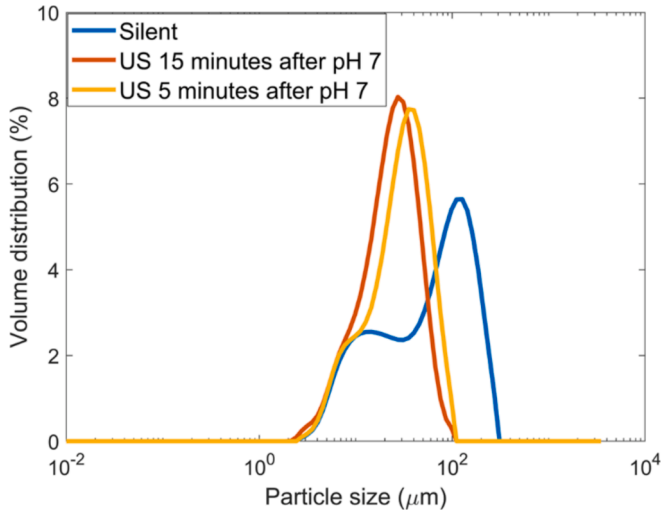

Fig. 8. Particle size volume distribution at different sonication durations.

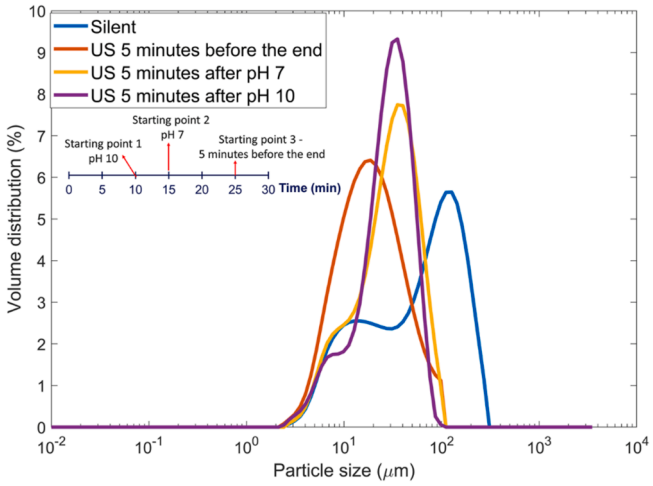

Fig. 9. Particle size volume distribution at different sonication starting points.

Table 3
Average particle size and filtration time.

Sonication Condition		Average Filtration Time (s)	Dx10 (μm)	Dx50 (μm)	Dx90 (μm)	Span
0 W/L (Silent condition)		16	10.23	65.09	167.7	2.42
Power[1]	8.4 W/L	117	10.34	29.05	61.13	1.75
	22.6 W/L	57	8.18	24.17	49.88	1.73
	36.3 W/L	141	6.74	20.47	44.00	1.82
Duration[2]	15 mins after pH 7	57	8.18	24.17	49.88	1.73
	5 mins after pH 7	58	8.53	30.48	62.90	1.78
	5 mins before the end	239	7.20	19.05	49.98	2.25
Starting point[3]	5 mins after pH 7	58	8.53	30.48	62.90	1.78
	5 mins after pH 10	34	9.47	29.87	54.17	1.50

[1] With the same duration of 15 min and the same sonication starting point (when pH reached 7);
[2] With the same sonication power 22.6 W/L and the same sonication starting point (pH 7);
[3] With the same sonication power of 22.6 W/L and duration of 5 min.

experiments was chosen as 100:7.5. Table 1 listed the detailed flow conditions like flow rates, flow ratios, and residence time. After the two reactants mixed and continued flowing for 8 min, there was no nucleation observed by the naked eye and the filter membrane placed in the end did not collect any nuclei. Then the amount of HCl was increased to give a flow ratio of 100:8 and further to 100:8.5, but still no nuclei were obtained. pH was tested by collecting the outflowing mixture in a centrifuge tube and measuring the pH via the pH probe. pH measurement results are given in Fig. 10. One can see at the flow ratio of 100:8.0, pH of the mixture reached ca. 6 meaning that the mixture was already neutralized. Even more HCl in the mixture at the flow ratio of 100:8.5 did not induce nucleation. The main difference between batch and continuous experiments was that the mixture of two reactants was mechanically stirred in the batch reactor, while it was flowing in a laminar fashion in the continuous reactor. The pH results in the flow experiments were comparable with those in the batch experiments because the outflowing mixture was mixed well by the insertion of the pH probe.

Following the silent flow experiments as a reference, ultrasound was introduced to explore the possibility of inducing nucleation. The conditions tested for this set of experiments varied on two aspects: a) flow

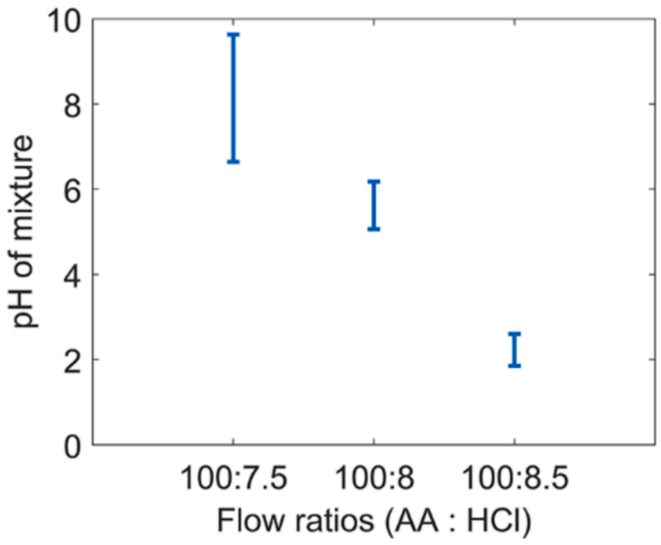

Fig. 10. pH of mixture at different flow ratios of aa and hcl. error bars represent the standard deviation of three identical experiments.

ratio of AA and HCl and b) sonication power. Ultrasound was turned on when HCl entered the flow reactor (AA was already in there) and at the same time, the timing of induction time began. Fig. 11 shows the induction time under ultrasound at different flow ratios. The induction time for flow ratio of 100:7.5, 100:8.0, and 100:8.5 was 83, 141, and 153 s, respectively, and the average of the three was 126 s. The induction time normalized by the residence time varied from 3 to 6 times the residence time, yielding an average of 5 times the residence time. When taking the standard deviation into account, there was not much difference in induction time under different flow ratios when applying the same sonicated conditions. Combined with the above pH results, pH reached ca. 10 which was a reasonable pH enabling nucleation based on the findings in batch experiments. Therefore, the amount of HCl did not affect the induction time a lot as long as pH reached below 10 when ultrasound was present in flow experiments.

3.2.2. *Induction time at different sonication powers*

The application of ultrasound initiated crystallization within the small flow reactor which was not achieved in silent conditions. The effects of sonication power were studied. Fig. 12 shows the induction time under different sonication powers while the same flow ratio of 100:7.5 was used. One can see that as the sonication power increased from 93.4 W/L to 216.5 W/L, the induction time reduced slightly from 87 s to 72 s, suggesting the powerful sonication 216.5 W/L may not be preferred from the perspective of rational energy use. As described in Table 2, electrical powers of 5 W, 10 W, and 15 W were applied to generate sonication powers of 93.4, 165.9, and 216.5 W/L, respectively. A low electrical power around or below 5 W is sufficient to induce nucleation in such a small flow reactor.

3.2.3. *Particle analysis*

Based on the result from batch experiments that ultrasound will not change the crystal form, FTIR analysis was not performed for the crystals collected in continuous experiments. Particle shape and size distribution were analyzed aiming to study the formation mechanism of the porous particles. As shown in Fig. 13, one can see the crystals appeared like overlapped and interlaced crystal strips. Compared to the SEM images from 30-minute batch experiments (Fig. 5), the crystals here were in a very early stage of crystallization. All crystals were fresh nuclei, without sufficient further growth or agglomeration. This was consistent with the PSD result (Fig. 14) that the peak was located at the size of 16 μm and the crystal sizes presented a very uniform and narrow distribution. It conveys the information that many small nuclei agglomerated into large particles over time. The agglomeration and deagglomeration degree are the key factors for the final product size and size distribution in continuous process.

3.3. *Discussion on applying ultrasound to intensify industrial crystallization of the aromatic amine*

The experimental findings on the application of ultrasound in reactive crystallization of the aromatic amine are summarized in Table 4. The objectives set out in this work were accomplished, especially revealing that ultrasound will intensify the reactive crystallization of this aromatic amine without changing the crystal form or shape. However, there are still several considerations that need to be made going further for applying ultrasound to this process.

First of all, it was found that in a batch mode, ultrasound influenced the crystallization yields and product sizes mainly by increasing the crystallization rate and deagglomeration. Secondary nucleation, crystal growth, agglomeration, and deagglomeration are all affected, but which mechanism is dominant is not clear. The pH value at which ultrasound is started, also affected this reactive crystallization process because it is driven by the decrease in pH. However, lacking of in-process analysis made it difficult to understand the 'Black-box', which made it difficult to answer at which point to introduce ultrasound and keep it on for how long would be best. A kinetics study with the aid of PAT tools should be

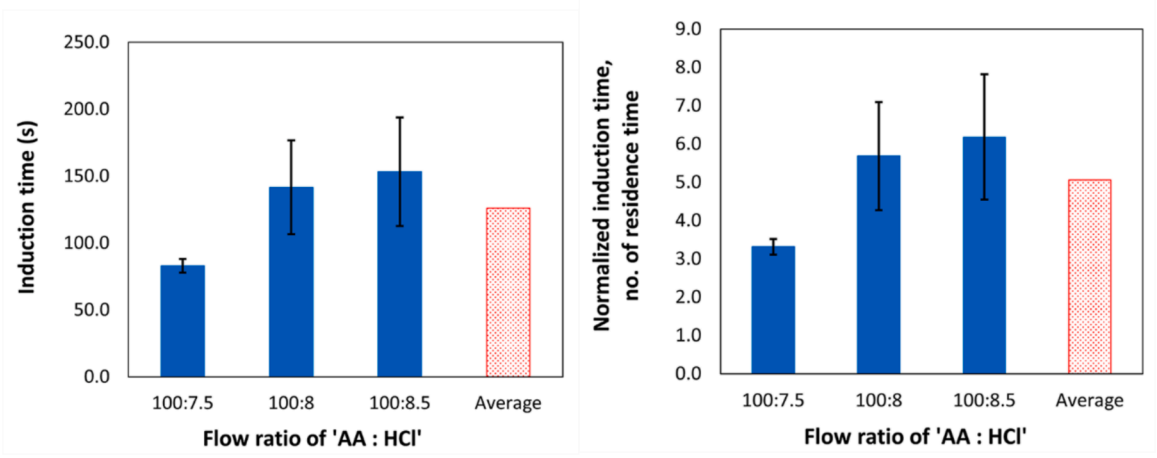

Fig. 11. Induction time for sonicated experiments at different flow ratios of AA and HCl. Sonication power: 165.9 W/L; residence time: 25 s. Left) Induction time in seconds. Right) Residence time normalized induction time. Error bars represent the standard deviation of three identical experiments.

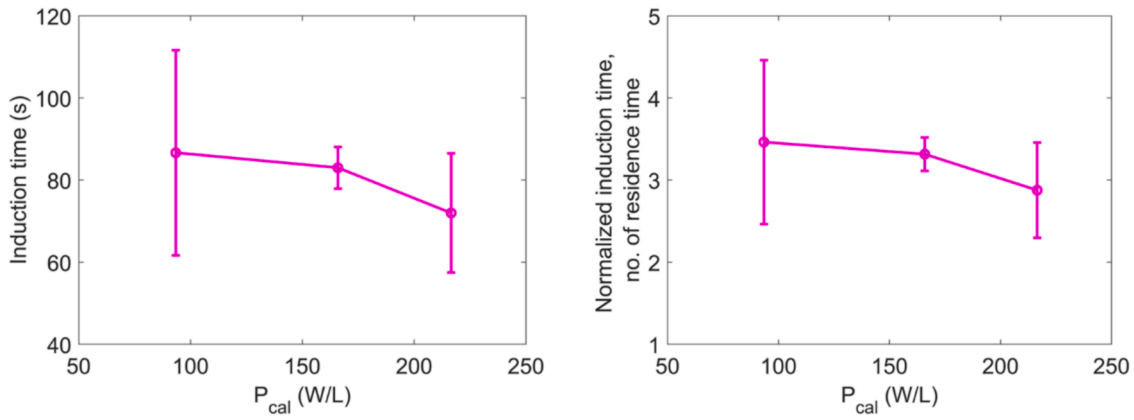

Fig. 12. Induction time for sonicated experiments at different sonication powers (Calorimetric power P_{cal}). Volume based flow ratio of AA and HCl: 100:7.5; residence time: 25 s. Left) Induction time in seconds. Right) Residence time normalized induction time. Error bars represent the standard deviation of three identical experiments.

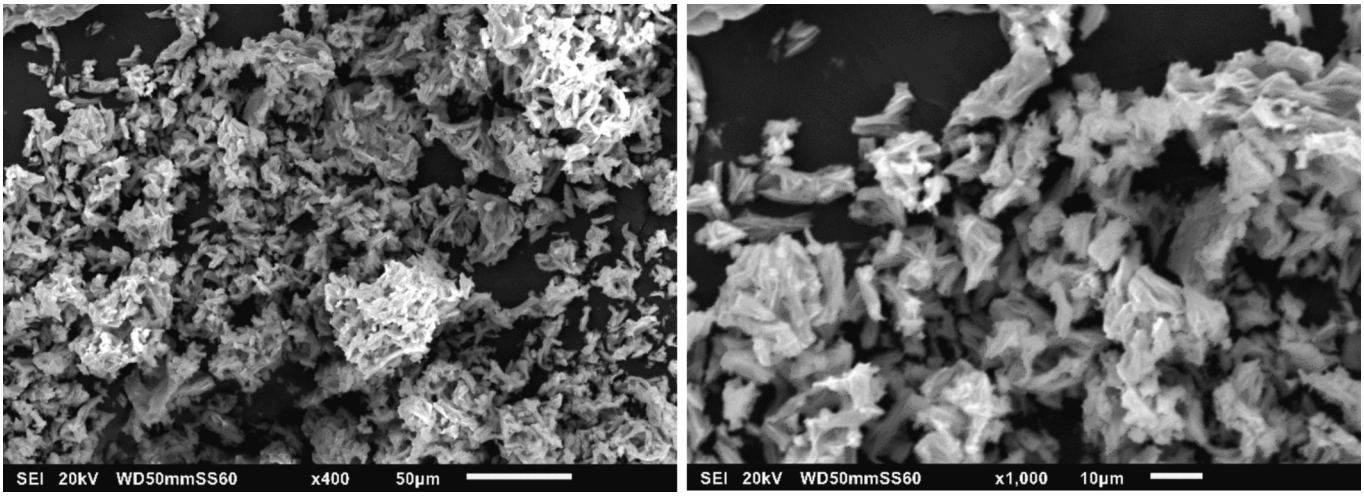

Fig. 13. SEM images of crystals collected in flow experiments. Sonication power: 165.9 W/L; flow ratio: 100:7.5; residence time: 25 s.

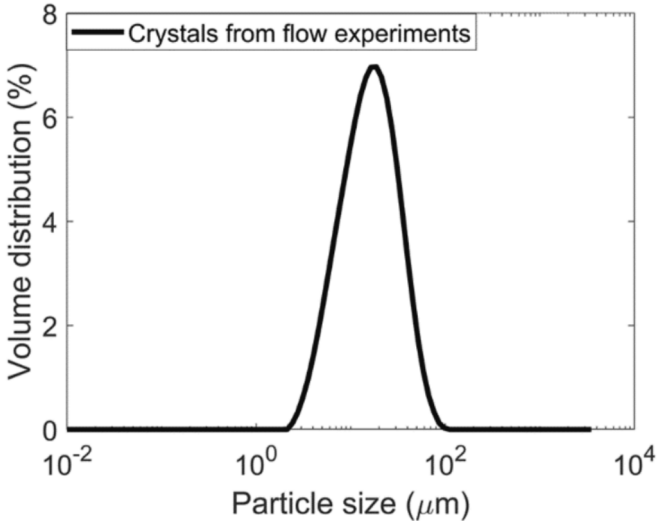

Fig. 14. Particle size volume distribution of crystals collected in flow experiments. Sonication power: 165.9 W/L; flow ratio: 100:7.5; residence time: 25 s.

considered to understand the mechanism behind the intensification and will help apply ultrasound to control the desired product sizes.

Second, this study pointed out that applying the appropriate sonicated conditions could initiate the nucleation of AA in flow conditions which did not happen in a silent flow condition. This suggests that ultrasound can be considered as a replacement for the seeding technique. An in-depth study on whether ultrasound can work as seeding in the flow crystallization of compound AA is ongoing. Further research on different flow and sonicated conditions, such as changing the residence time, less HCl, lower sonication power, and trying pulsed ultrasound, will give an in-depth idea of applying ultrasound in this flow system.

Additionally, the vacuum filtration in continuous experiments of this work was only applied for filtering the outflowing slurry and collecting samples. To shift toward continuous manufacturing, another challenge is the continuous filtration and drying process which should be coupled together after the crystallization. Some continuous filtration setups suitable for continuous manufacturing of APIs have been reported [33–35]. Therefore, future studies will focus on coupling the sonicated and continuous nucleator with another type of crystallizer for nuclei growth as well as further continuous filtration, which is expected to intensify the industrial crystallization process and also control the final particle properties to achieve good product quality.

Table 4
Summary of the benefits of applying ultrasound in the studied crystallization system.

Applied process	Benefits of ultrasound	Referred data	Increased yield (%)	D50 (μm)	Span	Ultrasound applied Power (W/L)	Ultrasound applied Duration (min)	Ultrasound applied Starting point
In batch process	1. increasing yields	Fig. 6	73.3	–	–	8.4	15	pH 7
			75.5	–	–	22.6	15	pH 7
			75.5	–	–	36.3	15	pH 7
	2. control particle size and size distribution	Fig. 7	–	29.05	1.75	8.4	15	pH 7
			–	24.17	1.73	22.6	15	pH 7
			–	20.47	1.82	36.3	15	pH 7
			–	19.05	2.25	22.6	5	End[1]
		Fig. 9	–	30.48	1.78	22.6	5	pH 7
			–	29.87	1.50	22.6	5	pH 10
In continuous process	3. enabling nucleation	Fig. 11 Fig. 12 Induction time measurements						

[1] Increased yield (%) is calculated as an increased ratio compared to silent experiments.
[2] 5 minutes before the end of experiments (the final 5 min).

4. Conclusions and Prospects

In this work, the application of ultrasound on reactive crystallization of an aromatic amine was studied in both a batch and continuous process, focusing on the effects on the crystallization process and the final particle properties. From the batch experiments, compound AA appeared stable under ultrasound and the crystal form did not change. The sonicated products had a similar morphology as the products obtained in silent experiments. The notable effects were mainly related to yields and particle sizes. The yields of sonicated experiments increased by 84% compared to those of the silent experiments. The particle sizes were reduced on average and a unimodal distribution was obtained under different conditions of ultrasound, specifically, a) more powerful sonication resulted in smaller particle sizes, and sonicated particles reached a minimum size of around 25 μm at the sonication power of 36.3 W/L; b) smaller particle sizes were obtained after longer sonication time of 15 min compared to 5 min; c) with the same sonication power and time, starting sonication at an earlier stage (pH of 10) led to a product with the narrowest span of 1.50 and a peak size of 35 μ m. The nucleation process and de-agglomeration were predicted to be the most impacted stages during the reactive crystallization of AA. Ultrasound was considered to enhance the nucleation rate at the early stage and boost de-agglomeration at the later stage of the whole crystallization process. Additionally, the filterability was tested by comparing the filtration time under the same slurry volume and filter conditions. This set of filtration experiments suggested that the presence of fine particles in the sonicated experiments slowed down the downstream filtration. Still, ultrasound could be able to optimize this process by producing a more uniform distribution of particle sizes.

According to the continuous experiments, a major advantage of ultrasound on continuous crystallization of AA was to enable nucleation which silent flow cannot. The crystal nuclei collected in flow experiments presented a uniform morphology and particle size distribution, implying the introduction of ultrasound can be a good technique for inducing nucleation to take up the role of seeding. Insights on sonication power can guide energy-efficient ultrasound integration in continuous nucleation. Further efforts on ultrasound-assisted continuous crystallization will focus on designing a complete process, combining continuous crystallization with the downstream continuous filtration and drying process.

CRediT authorship contribution statement

Biyu Zhang: Writing – review & editing, Writing – original draft, Visualization, Methodology, Investigation, Data curation, Conceptualization. **Ida Ådnebergli:** Writing – review & editing, Methodology, Data curation. **Georgios D. Stefanidis:** Writing – review & editing, Supervision, Methodology, Funding acquisition. **Tom Van Gerven:** Writing – review & editing, Supervision, Resources, Project administration, Methodology, Funding acquisition, Conceptualization.

Declaration of competing interest

The authors declare that they have no known competing financial interests or personal relationships that could have appeared to influence the work reported in this paper.

Acknowledgements

The research leading to these results has received funding from the European Union's Horizon research and innovation programmes under Grant Agreement No. 101058279 (SIMPLI-DEMO). This publication reflects only the authors' view, exempting the Community from any liability. Project website: https://simpli-demo.eu/.

We are thankful to GE HealthCare (Lindesnes, Norway) for their generous donation of the compound and the fruitful discussion on crystallization of this Aromatic Amine.

References

[1] R. Achermann, A. Košir, B. Bodák, L. Bosetti, M. Mazzotti, Process Performance and Operational Challenges in Continuous Crystallization: A Study of the Polymorphs of L-Glutamic Acid, Cryst. Growth Des. 23 (2023) 2485–2503, https://doi.org/10.1021/acs.cgd.2c01424.
[2] B.Y. Shekunov, P. York, Crystallization processes in pharmaceutical technology and drug delivery design, J. Cryst. Growth 211 (2000) 122–136, https://doi.org/10.1016/S0022-0248(99)00819-2.
[3] S. Diab, D.T. McQuade, B.F. Gupton, D.I. Gerogiorgis, Process Design and Optimization for the Continuous Manufacturing of Nevirapine, an Active Pharmaceutical Ingredient for HIV Treatment, Org. Process Res. Dev. 23 (2019) 320–333, https://doi.org/10.1021/acs.oprd.8b00381.
[4] C. Fang, W. Tang, S. Wu, J. Wang, Z. Gao, J. Gong, Ultrasound-assisted intensified crystallization of L-glutamic acid: Crystal nucleation and polymorph transformation, Ultrason. Sonochem. 68 (2020) 105227, https://doi.org/10.1016/j.ultsonch.2020.105227.
[5] N.J. Mozdzierz, Y. Lee, M.S. Hong, M.H.P. Benisch, M.L. Rasche, U.E. Tropp, M. Jiang, A.S. Myerson, R.D. Braatz, Mathematical modeling and experimental validation of continuous slug-flow tubular crystallization with ultrasonication-induced nucleation and spatially varying temperature, Chem. Eng. Res. Des. 169 (2021) 275–287, https://doi.org/10.1016/j.cherd.2021.03.026.
[6] A. Vancleef, T. Van Gerven, L.C.J. Thomassen, L. Braeken, Ultrasound in Continuous Tubular Crystallizers: Parameters Affecting the Nucleation Rate, Crystals 11 (2021) 1054, https://doi.org/10.3390/cryst11091054.
[7] B. Gielen, T. Claes, J. Janssens, J. Jordens, L.C.J. Thomassen, T. Van Gerven, L. Braeken, Particle Size Control during Ultrasonic Cooling Crystallization of Paracetamol, Chem. Eng. Technol. 40 (2017) 1300–1308, https://doi.org/10.1002/ceat.201600647.
[8] K.A. Ramisetty, K.V. Kumar, Å.C. Rasmuson, Advanced Size Distribution Control in Batch Cooling Crystallization Using Ultrasound, Org. Process Res. Dev. 23 (2019) 935–944, https://doi.org/10.1021/acs.oprd.9b00033.
[9] J. Jordens, B. Gielen, C. Xiouras, M.N. Hussain, G.D. Stefanidis, L.C.J. Thomassen, L. Braeken, T. Van Gerven, Sonocrystallisation: Observations, theories and

guidelines, Chem. Eng. Process. - Process Intensif. 139 (2019) 130–154, https://doi.org/10.1016/j.cep.2019.03.017.
[10] O. Narducci, A.G. Jones, Seeding in situ the cooling crystallization of adipic acid using ultrasound, Cryst. Growth Des. 12 (2012) 1727–1735, https://doi.org/10.1021/cg200677p.
[11] J. Zhao, P. Yang, J. Fu, Y. Wang, C. Wang, Y. Hou, Y. Shi, K. Zhang, W. Zhuang, H. Ying, Polymorph control by designed ultrasound application strategy: The role of molecular self-assembly, Ultrason. Sonochem. 89 (2022) 106118, https://doi.org/10.1016/j.ultsonch.2022.106118.
[12] M.N. Hussain, J. Jordens, S. Kuhn, L. Braeken, T. Van Gerven, Ultrasound as a tool for polymorph control and high yield in flow crystallization, Chem. Eng. J. 408 (2021) 127272, https://doi.org/10.1016/j.cej.2020.127272.
[13] U.N. Hatkar, P.R. Gogate, Ultrasound Assisted Cooling Crystallization of Sodium Acetate, Ind. Eng. Chem. Res. 51 (2012) 12901–12909, https://doi.org/10.1021/ie202220q.
[14] J. Jordens, B. Gielen, L. Braeken, T. Van Gerven, Determination of the effect of the ultrasonic frequency on the cooling crystallization of paracetamol, Chem. Eng. Process. Process Intensif. 84 (2014) 38–44, https://doi.org/10.1016/j.cep.2014.01.006.
[15] M.A. McDonald, H. Salami, P.R. Harris, C.E. Lagerman, X. Yang, A.S. Bommarius, M.A. Grover, R.W. Rousseau, Reactive crystallization: a review, React, Chem. Eng. 6 (2021) 364–400, https://doi.org/10.1039/D0RE00272K.
[16] Z. Guo, A.G. Jones, N. Li, The effect of ultrasound on the homogeneous nucleation of BaSO4 during reactive crystallization, Chem. Eng. Sci. 61 (2006) 1617–1626, https://doi.org/10.1016/j.ces.2005.09.009.
[17] Z. Guo, A.G. Jones, H. Hao, B. Patel, N. Li, Effect of ultrasound on the heterogeneous nucleation of BaSO4 during reactive crystallization, J. Appl. Phys. 101 (2007) 54907, https://doi.org/10.1063/1.2472652.
[18] B. Chen, S. Bao, Y. Zhang, C. Li, Reactive crystallization of ammonium polyvanadate from vanadium-bearing solution assisted by efficient ultrasound irradiation: Crystallization characteristics and growth process, J. Mater. Res. Technol. 25 (2023) 667–680, https://doi.org/10.1016/j.jmrt.2023.05.250.
[19] Y. Ma, Z. Li, P. Shi, J. Lin, Z. Gao, M. Yao, M. Chen, J. Wang, S. Wu, J. Gong, Enhancing continuous reactive crystallization of lithium carbonate in multistage mixed suspension mixed product removal crystallizers with pulsed ultrasound, Ultrason. Sonochem. 77 (2021) 105698, https://doi.org/10.1016/j.ultsonch.2021.105698.
[20] P. Adamou, E. Harkou, A. Villa, A. Constantinou, N. Dimitratos, Ultrasonic reactor set-ups and applications: A review, Ultrason. Sonochem. 107 (2024) 106925, https://doi.org/10.1016/j.ultsonch.2024.106925.
[21] V.V. Banakar, S.S. Sabnis, P.R. Gogate, A. Raha, Saurabh, Ultrasound assisted continuous processing in microreactors with focus on crystallization and chemical synthesis: A critical review, Chem. Eng. Res. Des. 182 (2022) 273–289, https://doi.org/10.1016/j.cherd.2022.03.049.
[22] J. Jordens, N. De Coker, B. Gielen, T. Van Gerven, L. Braeken, Ultrasound precipitation of manganese carbonate: The effect of power and frequency on particle properties, Ultrason. Sonochem. 26 (2015) 64–72, https://doi.org/10.1016/j.ultsonch.2015.01.017.
[23] A. Vancleef, S. Seurs, J. Jordens, T. Van Gerven, L.C.J. Thomassen, L. Braeken, Reducing the induction time using ultrasound and high-shear mixing in a continuous crystallization process, Crystals 8 (2018) 326, https://doi.org/10.3390/cryst8080326.
[24] C.P.M. Roelands, J.H. ter Horst, H.J.M. Kramer, P.J. Jansens, Precipitation mechanism of stable and metastable polymorphs of L-glutamic acid, AIChE J. 53 (2007) 354–362, https://doi.org/10.1002/aic.11072.
[25] M.N. Hussain, J. Jordens, J.J. John, L. Braeken, T. Van Gerven, Enhancing pharmaceutical crystallization in a flow crystallizer with ultrasound: Anti-solvent crystallization, Ultrason. Sonochem. 59 (2019) 104743, https://doi.org/10.1016/j.ultsonch.2019.104743.
[26] M. Fujiwara, P.S. Chow, D.L. Ma, R.D. Braatz, Paracetamol Crystallization Using Laser Backscattering and ATR-FTIR Spectroscopy: Metastability, Agglomeration, and Control, Cryst. Growth Des. 2 (2002) 363–370, https://doi.org/10.1021/cg0200098.
[27] R.F. Contamine, A. Wilhelm, J. Berlan, H. Delmas, Power measurement in sonochemistry, Ultrason. Sonochem. 2 (1995) S43–S47, https://doi.org/10.1016/1350-4177(94)00010-P.
[28] T. Kimura, T. Sakamoto, J.-M. Leveque, H. Sohmiya, M. Fujita, S. Ikeda, T. Ando, Standardization of ultrasonic power for sonochemical reaction, Ultrason. Sonochem. 3 (1996) S157–S161, https://doi.org/10.1016/S1350-4177(96)00021-1.
[29] L.H. Thompson, L.K. Doraiswamy, Sonochemistry: Science and Engineering, Ind. Eng. Chem. Res. 38 (1999) 1215–1249, https://doi.org/10.1021/ie9804172.
[30] S. Kaur Bhangu, M. Ashokkumar, J. Lee, Ultrasound Assisted Crystallization of Paracetamol: Crystal Size Distribution and Polymorph Control, Cryst. Growth Des. 16 (2016) 1934–1941, https://doi.org/10.1021/acs.cgd.5b01470.
[31] S.R. Iyer, P.R. Gogate, Ultrasound assisted crystallization of mefenamic acid: Effect of operating parameters and comparison with conventional approach, Ultrason. Sonochem. 34 (2017) 896–903, https://doi.org/10.1016/j.ultsonch.2016.08.001.
[32] M.N. Hussain, S. Baeten, J. Jordens, L. Braeken, T. Van Gerven, Process intensified anti-solvent crystallization of o-aminobenzoic acid via sonication and flow, Chem. Eng. Process. - Process Intensif. 149 (2020) 107823, https://doi.org/10.1016/j.cep.2020.107823.
[33] N. Yazdanpanah, S.T. Ferguson, A.S. Myerson, B.L. Trout, Novel Technique for Filtration Avoidance in Continuous Crystallization, Cryst. Growth Des. 16 (2016) 285–296, https://doi.org/10.1021/acs.cgd.5b01231.
[34] Y.C. Liu, A. Domokos, S. Coleman, P. Firth, Z.K. Nagy, Development of Continuous Filtration in a Novel Continuous Filtration Carousel Integrated with Continuous Crystallization, Org. Process Res. Dev. 23 (2019) 2655–2665, https://doi.org/10.1021/acs.oprd.9b00342.
[35] W. Wu, R. Sayin, K. Shvedova, S.C. Born, C.J. Testa, S.S. Yeole, A.S. Censullo, A. K. Srivastava, A. Ramnath, C. Hu, B. Takizawa, T.F. O'Connor, X.B. Yang, S. Ramanujam, S. Mascia, A Continuous Rotary Filtration for the Separation and Purification of an Active Pharmaceutical Ingredient, Org. Process Res. Dev. (2023), https://doi.org/10.1021/acs.oprd.3c00263.